*Anal. Chem.* **2002,** *74,* 5017−5026

# A Monte Carlo Model for Studying the Microheterogeneity of Trace Elements in Reference Materials by Means of Synchrotron Microscopic X-ray Fluorescence

Lieven Kempenaers,*,† Koen Janssens,*,† Laszlo Vincze,† Bart Vekemans,† Andrea Somogyi,‡ Michael Drakopoulos,‡ Alexandre Simionovici,‡ and Freddy Adams†

*Department of Chemistry, University of Antwerp, Universiteitsplein 1, B-2610 Antwerp, Belgium, and European Synchrotron Radiation Facility, BP 220, F-38043 Grenoble, Cedex, France*

**Synchrotron micro-XRF, a trace-level microanalytical method, allows quantitative study of the nature and degree of heterogeneity of inorganic trace constituents in solid materials with a homogeneous matrix. In this work, the standard reference materials NIST SRM 613, Trace Elements in 1 mm Glass Wafers, and NIST SRM 1577a, Trace Elements in Bovine Liver, are examined at the 10−100-ng mass level using X-ray beams of 5−150 $\mu$m in diameter. A procedure based on a large number of repeated analyses of small absolute amounts of the SRMs allows calculation of the minimal representative mass of the standard. The microheterogeneity of both NIST SRM 613 and NIST SRM 1577a was investigated with the aim of evaluating their suitability as reference materials for trace-level microanalytical techniques. A Monte Carlo simulation model was constructed for both homogeneous and heterogeneous materials to elucidate the dependence of the calculated minimal representative mass on the total analyzed mass in the case of materials that show strongly heterogeneous features at the microscopic level.**

A trend in inorganic instrumental analytical chemistry has been the development of microscopic equivalents of established analytical techniques. Usually, these microbeam methods are able to analyze (microscopically) small parts of a large solid specimen. Examples of techniques that are able to provide trace element information are: laser ablation inductively coupled plasma mass spectrometry (LA-ICPMS);[1−4] laser-induced breakdown spectrometry (LIBS);[1,5,6] microscopic X-ray fluorescence analysis ($\mu$-XRF),[7−9] and proton-induced X-ray emission ($\mu$-PIXE).[10,11] The fact that the techniques yield information on trace element concentrations in well-defined locations on the surface of a material makes them very powerful investigation techniques for heterogeneous materials of industrial, geological, biological, or environmental nature. With many of these methods, sample preparation can largely be dispensed with, which is advantageous in terms of speed and ease of use.

Although the number of reports on the successful application of these methods in a variety of fields is steadily increasing, the availability of microscopically homogeneous reference materials, certified for the presence of one or more trace elements inside commonly occurring matrixes (e.g., polymers, glass, and aluminum), is not increasing at the same rate.

As a result of the lack of suitable reference materials (RMs), calibration of many microanalytical instruments is being performed by means of bulk reference materials that were never intended for this purpose. In these bulk standards, usually the abundance of one or more trace constituents is certified; however, these certified values can only be relied upon when a sufficiently large quantity of the RM in question is analyzed. An example is NIST SRM 1577a, Trace Elements in Bovine Liver, certified for the elements Cd, Cu, Fe, Hg, Mn, Pb, Rb, Se, and Zn of which, according to the certificate, a minimum amount of 250 mg must be used.[12]

It appears that, for a number of elements in a specific standard, the "minimal representative mass" has been rather arbitrarily determined in the past or has been estimated very conservatively so that the recommended values are (significantly) higher than the estimated minimal mass one arrives upon when the micro-

† University of Antwerp.

‡ European Synchrotron Radiation Facility.

(1) Moenke-Blankenburg, L. *Laser Microanalysis*; Wiley: New York, 1989; Vol. 105.

(2) Jeffries, T. E. In *Nondestructive Elemental Analysis*; Alfassi, Z. B., Ed.; Blackwell Science: Oxford, U.K., 2001; Chapter 3, pp 115−150.

(3) Houk, R. S. *Laser Ionization Techniques for Analytical Mass Spectrometry in Analytical Applications of Lasers*; Wiley: New York, 1986.

(4) Hoffmann, E.; Ludke, C.; Stephanowitz, H. *Fresenius' J. Anal. Chem.* **1996**, *355*, 900−903.

(5) Vadillo, J. M.; Palanco, S.; Romero, M. D.; Laserna, J. J. *Fresenius' J. Anal. Chem.* **1996**, *355*, 909−912.

(6) Radziemski, L. J.; Solarz, R. W.; Paisner, J. A. *Laser spectroscopy and its applications*; Dekker: New York, 1987.

(7) Janssens, K.; Vincze, L.; Rubio, J.; Adams, F. *J. Anal. At. Spectrom.* **1994**, *9*, 151−157.

(8) Janssens, K.; Vincze, L.; Adams, F.; Jones, K. W. *Anal. Chim. Acta* **1993**, *283*, 98−119.

(9) Janssens, K.; Vincze, L.; Vekemans, B.; Aerts, A.; Adams, F.; Jones, K. W.; Knöchel, A. *Microchim. Acta* **1996**, *13*, 87−115.

(10) Alfassi, Z. B. *Chemical Analysis by Nuclear Methods*; Wiley: New York, 1994.

(11) Johansson, S. A. E.; Campbell, J. L. *PIXE: A Novel Technique for Elemental Analysis*; Wiley: New York, 1988.

(12) National Institute of Standards and Technology, Certificate of Analysis, Standard Reference Material 1577a 'Trace Elements in Bovine Liver'; Washington, DC, April 1972.

10.1021/ac025662g CCC: $22.00 
Published on Web 08/22/2002

heterogeneity of each element in the material is properly investigated.

Pauwels and Vandecasteele recommended that microheterogeneity studies are performed with small subvolumes or masses.[13] This recommendation was put into practice by Kempenaers et al.,[14] who presented a procedure for determining the microheterogeneity of existing reference materials on the basis of large series of individual analyses of very small subsamples (100-ng mass level) by means of synchrotron-based $\mu$-XRF. Since X-ray beams of 5−150-$\mu$m diameter were used to irradiate traces present at the 10−100 $\mu$g/g level in 100-$\mu$m-thick films, analyte masses were irradiated that are of the same order as those typically sampled or ablated during, for example, LA-ICPMS or $\mu$-PIXE determinations. The measurements involve an extensive series of analyses, performed under identical conditions at different locations on the material. Also, some attention was devoted to the repeatability of this microheterogeneity procedure and the factors that influence it.[15] An important factor determining this minimal representative mass is the abundance (if any) and mass distribution of "nuggets" throughout the RM, i.e., grainlike microinclusions where the local concentration of trace metals is significantly higher than in the matrix of the RM.[16]

To investigate in a systematic and quantitative manner the effects on the repeatability of the procedure of the overall abundance, average enrichment, and size/mass distribution of the inclusions relative to the matrix, a Monte Carlo simulation model was developed to simulate the response of materials of variable degree and type of (micro)heterogeneity when subjected to an extensive series of repeated analyses at the 10−100-ng mass level.

In this paper, a short description of this simulation model will be given for the case of both homogeneous and heterogeneous materials. Results of the model calculations will be compared to experimental data from two references materials having distinctly different microheterogeneity characteristics: the (more) homogeneous reference material NIST SRM 613, Trace Elements in Glass, and the (more) heterogeneous material NIST SRM 1577a, Trace Elements in Bovine Liver.

## EXPERIMENTAL SECTION

For the microprobe experiments, the $\mu$-XRF instrument installed at the ID18F end station of the European Synchrotron Radiation Facility (ESRF, Grenoble, France)[17] and the $\mu$-XRF instrument at beamline L of the Hamburg Synchrotron Laboratory (HASYLAB, Hamburg, Germany) were employed.[9] A number of instrumental characteristics of both facilities are listed in Table 1.

During the experiments, (quasi-)monochromatic (ESRF, 21 keV and HASYLAB, 17.5 keV) or polychromatic (HASYLAB, 5−50 keV) X-ray microbeams were employed to irradiate a small area of the sample. The sample was positioned at 45° to the incoming beam. The specimen is viewed by a horizontally mounted microscope equipped with a CCD camera, and the emerging fluorescent/scattered photons were collected by an energy-dispersive solid-state detector at 90° to the beam. Figure 1 represents the monochromatic experimental setup at ESRF-ID18F. In this setup, X-ray beams of different cross sections and compatible total intensities were generated by placing a compound refractive lens (CRL)[18] at different positions relative to the sample (Table 1). The intensity of the primary X-ray beam was monitored at three positions, by two ionization chambers and a PIN diode (see Figure 1). For thin foil samples, the detected X-ray fluorescence intensities are proportional to the irradiated mass of the elements in question, while the scatter background intensity is a measure of the total irradiated mass.

Table 1. Synchrotron $\mu$-XRF Instrumental Conditions for Beam Line ID18F at ESRF (Grenoble, France) and Beam Line L at HASYLAB (Hamburg, Germany)

| | ESRF-ID18F | HASYLAB (beamline L) | |
|---|---|---|---|
| X-ray source | monochromatic (21 keV) | polychromatic (1−80 keV) | wide band-pass (17.5−18.0 keV) |
| X-ray optics | compound refractive lens (CRL) | straight capillary | cross-slits |
| beam size | | | |
| 1 | 4 × 7 $\mu$m$^2$ | | |
| 2 | 5 × 8 $\mu$m$^2$ | | |
| 3 | 18 × 20 $\mu$m$^2$ | | |
| 4 | | 20 × 20 $\mu$m$^2$ | |
| 5 | 43 × 44 $\mu$m$^2$ | | |
| 6 | 90 × 96 $\mu$m$^2$ | | |
| 7 | | | 120 × 150 $\mu$m$^2$ |
| detector | Si(Li) | HPGe | Si(Li) |
| rel detection limit ($\mu$g/g) | 0.01−0.1 | 1−10 | 0.03−0.3 |

To study the microheterogeneity of a material, the sample, in the form of a 1-mm-thick wafer (NIST SRM 613) or a self-supporting film of thickness of ∼120 $\mu$m (NIST SRM 1577a) was moved in a regular pattern through the primary X-ray beam. XRF spectra are collected from a large number of locations, typically 441/sample, e.g., in a 21 × 21 grid. Per spectrum, a collection time of 50 s was chosen. In Figure 2a, a schematic view is plotted of a sample irradiated with an X-ray beam of 4 × 7 $\mu$m$^2$ cross section (see ESRF column in Table 1); the distance between the various irradiation positions usually was 150 $\mu$m.[14] With a sample thickness of ∼120 $\mu$m, a mass $m$ of 5 ng is irradiated. When performing repeated measurements at the same location on the sample, identical results are obtained, which indicates that the analysis is nondestructive for the applied method. For the evaluation of the resulting XRF spectra, the AXIL (Analysis of X-ray spectra by Iterative Least Squares) code was employed.[19]

Self-supporting disks of NIST SRM 1577a, Trace Elements in Bovine Liver, were prepared by pressing the material in pellets with a diameter of 1 cm and thickness of ∼120 $\mu$m.

As illustrated in Figure 2, a total of four series of analyses with increasing beam cross sections were performed on NIST SRM


(13) Pauwels, J.; Vandecasteele, C. *Fresenius' J. Anal. Chem.* **1993**, *345*, 121−123.

(14) Kempenaers, L.; Vincze, L.; Janssens, K. *Spectrochim. Acta, B* **2000**, *55*, 651−669.

(15) Kempenaers, L.; De Koster, C.; Van Borm, W.; Janssens, K. *Fresenius' J. Anal. Chem.* **2001**, *369*, 733−737.

(16) Kurfürst, U.; Pauwels, J.; Grobecker, K. H.; Stoeppler, M.; Muntau, H. *Fresenius J. Anal. Chem.* **1993**, *345*, 112−120.

(17) Somogyi, A.; Drakopoulos, M.; Vincze, L.; Vekemans, B.; Camerani, C.; Janssens, K.; Snigirev, A.; Adams, F. *X-Ray Spectrom.* **2001**, *30*, 242−252.

(18) Lengeler, B.; Schroer, C.; Tummler, J.; Benner, B.; Richwin, M.; Snigirev, A.; Snigireva, I.; Drakopoulos, M. *J. Synchrotron Radiat.* **1999**, *6*, 1153−1167.

(19) Van Espen, P.; Janssens, K.; Nobels, J. *Chemom, Intell. Lab. Syst.* **1986**, *1*, 109−114.

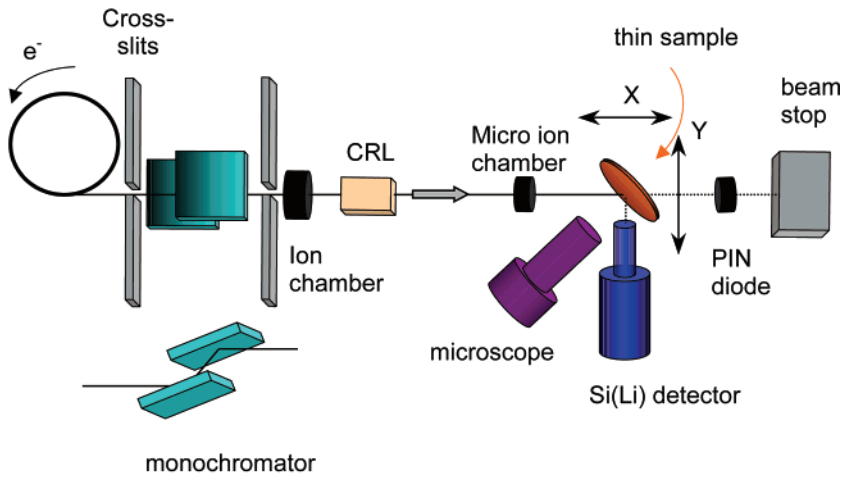


Figure 1. Synchrotron $\mu$-XRF setup at beam line ID18F of ESRF (Grenoble, France) showing micro X-ray optics, sample stage, and Si(Li) detector.

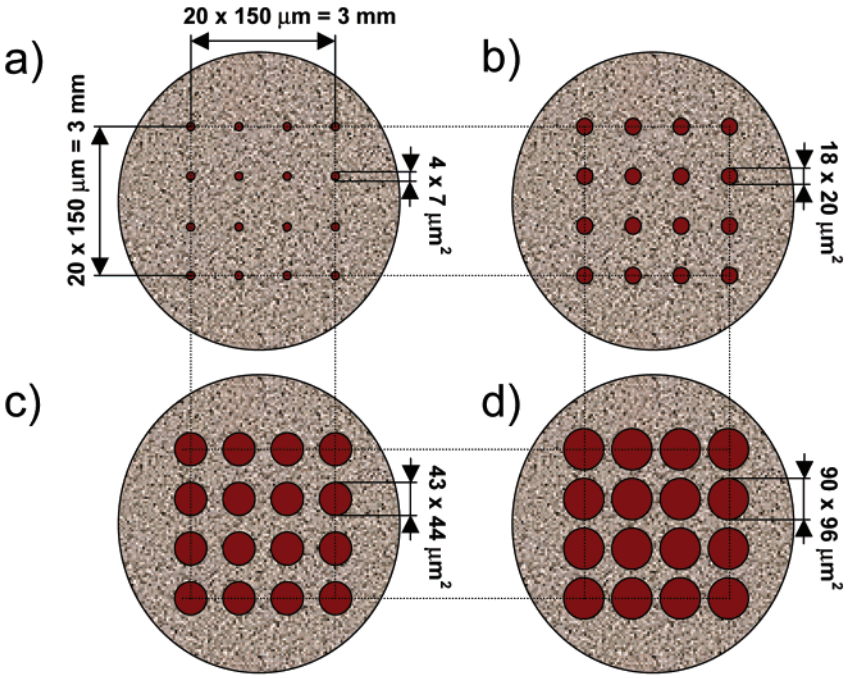


Figure 2. Schematic view of a sample irradiated with an X-ray beam with cross sections of (a) 4 × 7, (b) 18 × 20, (c) 43 × 44, and (d) 90 × 96 $\mu$m$^2$ at well-defined locations on the sample. A step size of 150 $\mu$m was employed during the ESRF-ID18F measurements.

1577a by means of the $\mu$-XRF setup at ESRF-ID18F. Thus, the analyzed mass $m$ varied from 5 to 1360 ng. Additionally, by means of an unfocused wide band-pass beam at HASYLAB beamline L, areas of 120 × 150 $\mu$m$^2$ were irradiated, corresponding to a mass of ~2.8 $\mu$g.

## THEORETICAL BACKGROUND

**Microheterogeneity Procedure.** The procedure for measuring the microheterogeneity of a given material by means of synchrotron $\mu$-XRF is described in detail in ref 14. Below, we briefly summarize the main points.

The measurements for calculating the minimal sampling mass $m_{\mathrm{min,5\%}}$, involve an extensive series of local analyses, performed under identical conditions at different locations on the material. The series of $n$ analyses result in $n$ independent estimates $c_i$ ($i$ = 1, ..., $n$) of the analyte concentration, distributed around an average value $<c>$ with a variance $s^2_{\mathrm{total},r}$. This variance is composed of an instrumental component $s^2_{\mathrm{instrument},r}$, a component due to counting statistics $s^2_{\mathrm{statistics},r}$, and the variance due to the heterogeneity of the material $s^2_{\mathrm{material},r}$:

$$s^2_{\mathrm{total},r} = (s^2_{\mathrm{instrument},r} + s^2_{\mathrm{statistics},r}) + s^2_{\mathrm{material},r} = s^2_{\mathrm{method},r} + s^2_{\mathrm{material},r} \quad (1)$$

The instrumental and the statistical components of $s^2_{\mathrm{total},r}$ can be grouped into $s^2_{\mathrm{method},r}$, the variance due to the analytical method.

When a microanalytical method is used, in many cases the sample surface, volume, or mass that is being analyzed can be chosen within certain limits (in this case by (de)focusing the primary X-ray beam onto a larger or smaller area and using the average signal produced). As the amount of material $m$ being analyzed decreases, the variation in the results due to the heterogeneity of the material becomes increasingly important;

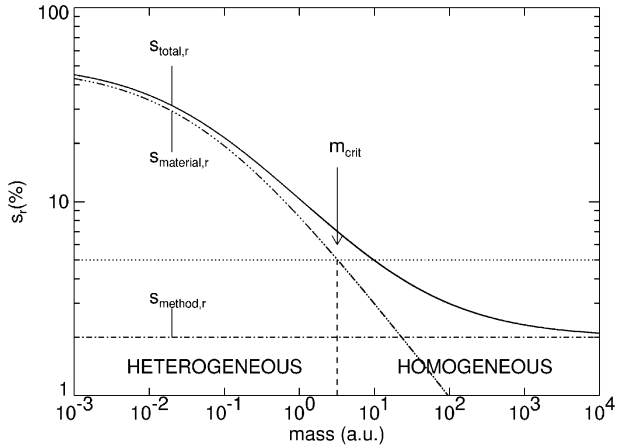


Figure 3. Decreasing value of $s_{total,r}$ and $s_{material,r}$ vs increasing analyzed mass $m$, ultimately resulting in a value equal to $s_{method,r}$.

conversely, as $m$ increases, averaging of the response results in decreasing values of $s^2_{total,r}$, until ultimately a value not significantly different from $s^2_{method,r}$ is reached.[20] As shown in Figure 3, the relative standard deviation due to the heterogeneity of the material $s_{material,r}$ decreases with increasing $m$; when $m$ exceeds a critical value $m_{crit}$, it will not differ significantly from zero. $m_{crit}$ is therefore the minimal representative mass above which a material appears to be homogeneous for a given method and type of analysis. There exist various ways of defining $m_{crit}$;[14] in this paper, the minimal representative mass ($m_{min,5\%}$) is defined as the mass that yields a value of 5% for $s_{material,r}$. The minimal mass can only be calculated at the 5% critical level when the measurement conditions are sufficiently repeatable, i.e., when $s_{method,r}$ is significantly lower than 5%.

Conventionally, the $s_{total,r}(m)$ versus $m$ graph is described by a power function:

$$s^2_{total,r}(m) = \left(\frac{1}{am^b + c}\right)^2 + s^2_{method,r} \qquad (2)$$

while to the $s_{material,r}(m)$ versus $m$ graph, a power law $s_{material,r}(m) = 1/(am^b + c)$ can be fitted. The fitting coefficient $a$ corresponds to the homogeneity factor $H_E$ [14] while the slope $b$ usually takes values close to 0.5. Once the coefficients $a$, $b$, and $c$ are known, it is possible to calculate the minimal representative mass $m_{min,5\%}$ corresponding to 5% relative material heterogeneity by using

$$m_{min,5\%} = \left(\frac{1}{0.5\%} - \frac{c}{a}\right)^{1/b} \qquad (3)$$

**Monte Carlo Simulation Model.** In a previous paper,[15] Kempenaers et al. already observed that the minimum representative mass $m_{min,5\%}$ is influenced by different parameters. In this context, a distinction can be made between the following three categories of reference materials: (a) homogeneous RMs, i.e., materials where the observed total variance $s^2_{total,r}$ does not significantly exceed the variance of the method $s^2_{method,r}$ employed to investigate it (Figure 4a); (b) normal heterogeneous RMs, i.e., materials featuring a $s^2_{total,r}$ significantly larger than $s^2_{method,r}$, but where the point-to-point variations of $c_i$ are distributed according to a Gaussian distribution with a spread equal to $s_{material,r}$ (Figure 4b); (c) nonnormal heterogeneous RMs, i.e., materials where $s^2_{total,r} > s^2_{method,r}$, but with a non-Gaussian distribution of the concentration throughout the material (Figure 4c).

In RMs belonging to category c, frequently the presence of nuggets (i.e., strongly localized enrichment areas) is observed.[13] These usually show a concentration distribution consisting of a Gaussian or non-Gaussian peak around the average concentration $<c>$ with one or more secondary maximums at high to very high $c$ value corresponding to the nuggets. Next to this type, other nonnormal concentration distributions can also be observed, e.g., due to the presence of less sharply defined enrichment areas of trace elements throughout the material.

To investigate the influence of the concentration distribution on the $m_{min,5\%}$ estimation, a Monte Carlo model was developed to simulate the response of materials with different degrees and types of microheterogeneity when subjected to the above-described series of repeated analyses.

In the Monte Carlo model, a material is considered to consist of a two-dimensional grid of $N_{total} = 3000 \times 3000$ subareas, each subarea measuring $3 \times 3\ \mu m^2$, which corresponds to a submass of ~1.3 ng when a sample thickness of 100 $\mu$m is assumed with a density of 1 g/cm$^3$ (Figure 5). The concentration in each volume element $c_i$ is normally distributed around a mean $<c>$ with variance $s^2_c$. In the MC model, one or more series of inclusions can be introduced, each series characterized by three parameters: (a) their area $S_{inclusion}$ (in units of subareas), (b) their number $N_{inclusion}$ throughout the material, and (c) their enrichment factor relative to the surrounding matrix: $E_{inclusion} = c_{inclusion}/<c>$. The probability for encountering an inclusion is therefore, $P = (N_{inclusion}S_{inclusion})/S_{total}$. The concentration distribution of the inclusions is Gaussian around a mean value $<c_{inclusion}>$ and having a spread $s_{inclusion}$. In Figure 5, a part of the Monte Carlo model is shown where several series of nuggets were included. Realistic values for $S_{inclusion}$ can be derived from elemental X-ray maps of minor and trace constituents of the materials being investigated. For example, in Figure 6a, Fe-enriched areas of ~15 × 20 $\mu m^2$ are visible in NIST SRM 1577a with $E$ in the range 1.2−1.7. To distinguish the areas with inclusions from the rest of the image, the mean concentration $<c_{map}>$ and its standard deviation $s_{map}$ are calculated. Two kinds of inclusions can be considered: "nuggets" and "islands". Nuggets show up in the maps as small areas (one or two pixels) having a concentration reading outside (i.e., above) the 3s confidence level [$<c_{map}> - 3s_{map}$, $<c_{map}> + 3s_{map}$]. Islands, on the other hand are larger areas with average concentration higher than $<c_{map}>$, but within the above-mentioned confidence interval. These more gradual concentration fluctuations are not random since series of adjacent pixels show similar (increased) $c$ values. The "islands" are characterized by their area $S_{island}$ and average enrichment factor $E_{island}$. In the simulation model, these structures are accounted for by randomly placing square-shaped inclusions of specific size and enrichment factor at various locations throughout the two-dimensional grid, giving rise to the spatial distribution shown in Figure 5. The enrichment value of a subarea that is part of two or more inclusions is set to the maximum enrichment factor of all involved inclusions. In this

(20) Danzer, K.; Küchler, L. *Talanta* **1977**, *24*, 561−565.

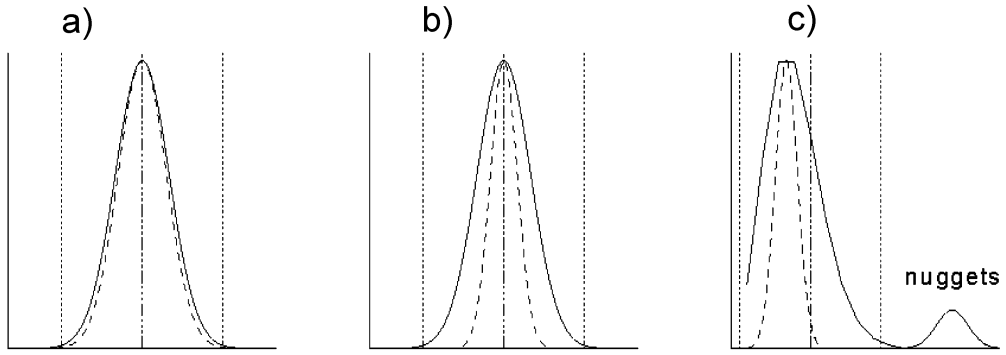


Figure 4. Three types of concentration distributions; (a) a Gaussian distribution with $s^2_{total,r} \cong s^2_{method,r}$, (b) a Gaussian distribution with $s^2_{total,r} > s^2_{method,r}$, and (c) a non-Gaussian distribution with nuggets. The dashed lines indicate a Gaussian distribution with standard deviation equal to $s_{method,r}$. In all cases, the $\pm 3s_{total,r}$ interval around the mean concentration value is indicated (dotted lines).

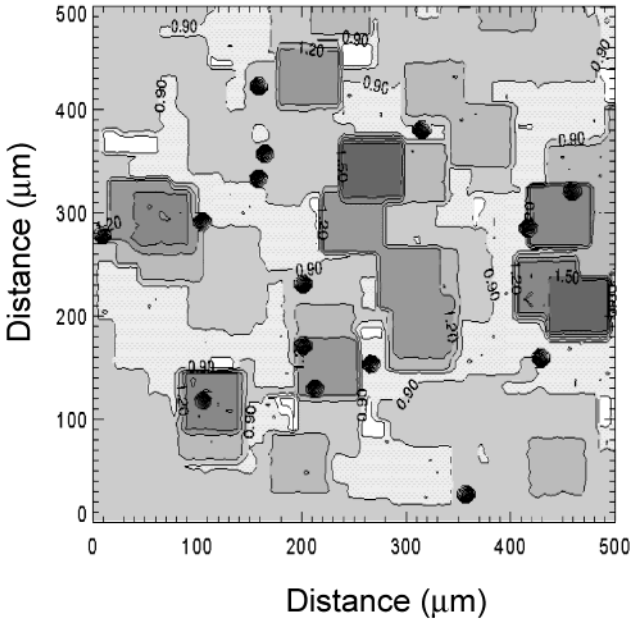


Figure 5. Part of a Monte Carlo simulation model including islands and nuggets with different values for the input parameters *P*, *E*, and *S*, covering a simulated area of 0.25 mm$^2$. White corresponds to the lowest *E* value while black is the highest *E* value.

way, overlapping islands can merge into larger islands of non-square shape.

After construction of the model on the basis of matrix and inclusion parameters derived from experimental data (see Figure 6), the equivalent of the procedure outlined in previous section is simulated: i.e., out of the $9 \times 10^6$ subareas, $21 \times 21$ areas in a squarelike arrangement (see Figure 2) are selected and the mean concentration per area and its standard deviation $s^{sim}_{total,r}$ calculated on the basis of individual $c_i$ values corresponding to each subarea.

To test the null hypothesis that the standard deviations of the experimental and simulated distributions $s^{exp}_{total,r}$ and $s^{sim}_{total,r}$ do not significantly differ from each other, i.e., that the population parameters $s^{exp}_{total,r}$ and $s^{sim}_{total,r}$ are equal, a Fisher's *F*-test can be performed at a certain statistical tolerance level (usually $\alpha = 0.05$ is employed) by using the condition

$$(s^{exp}_{total,r})^2/(s^{sim}_{total,r})^2 \leq F(\alpha, N_{exp}, N_{sim}) \quad (4)$$

where $N_{exp}$ and $N_{sim}$ are the degrees of freedom associated with the determination of $s^{exp}_{total,r}$ and $s^{sim}_{total,r}$, respectively. $F(\alpha, N_{exp}, N_{sim})$ is the partial integral of the corresponding *F* distribution; in the present case, where $N_{exp} = N_{sim} = 441$, the critical *F* value[21] equals 1.17 for $\alpha = 0.05$.

In what follows, first the procedure for determining $s_{instrumental}$ is outlined, after which the Monte Carlo model is employed to explain the observed variation of $s_{material}$ versus the analyzed mass *m* in the case of a homogeneous (type a) and a heterogeneous (type c) material.

## RESULTS AND DISCUSSION

**Estimation of $s_{method,r}$ from Replicate Analyses.** Before calculating the minimal representative mass $m_{min,5\%}$ of a certain element in the sample, the contribution to the total variation on the experimental readings due to the method $s_{method,r}$ must be estimated (see eq 1). As detailed elsewhere in greater detail,[2,14,23] in comparison to other microanalytical methods with trace-level sensitivity, $\mu$-XRF can be considered to be the least destructive: at the irradiated sample position; the matrix is neither evaporated or noticeably altered in (trace) composition (see also Figure 7) although more subtle changes such as modifications to the crystallographic structure (if any) or changes in valency of redox-sensitive elements can occur. Thus, $s_{method,r}$ can conveniently be determined experimentally by performing a series of repeated measurements *at the same location* on the sample.[22] The calculation of $s_{method,r}$ involves the estimation of $s_{instrument,r}$ and $s_{statistics,r}$. Considering that the concentration $c_i$ of a trace element in a given position is proportional to $I_{fl,i}/I_{scatter}$, the contribution of $s_{statistics,r}$ is calculated by considering the Poisson statistics on (a) the detected net fluorescent intensity $I_{fl,i}$, (b) the intensity of the background $B_{fl,i}$ below the fluorescent line, and (c) the integrated scatter intensity $I_{scatter}$ used for normalizing the data:

$$s^2_{statistics,r}(c_i) = s^2_{statistics,r}(I_{fl,i}/I_{scatter}) = s^2_{statistics,r}(I_{fl,i}) + s^2_{statistics,r}(I_{scatter}) \quad (5)$$

while $s_{instrument,r}$ is estimated from the difference between $s_{method,r}$

(21) Walker, H. M.; Lev, J. *Elementary Statistical Methods*, 3th ed.; Holt, Rinehart and Winston: New York, 1969; pp 358−361.
(22) Danzer, K. *Spectrochim. Acta B* **1984**, *39*, 949−954.
(23) Janssens, K., Adams, F., Rindby, A., Eds. *Microscopic X-ray Fluorescence Analysis*; Wiley: New York, 2000; pp 182−183.

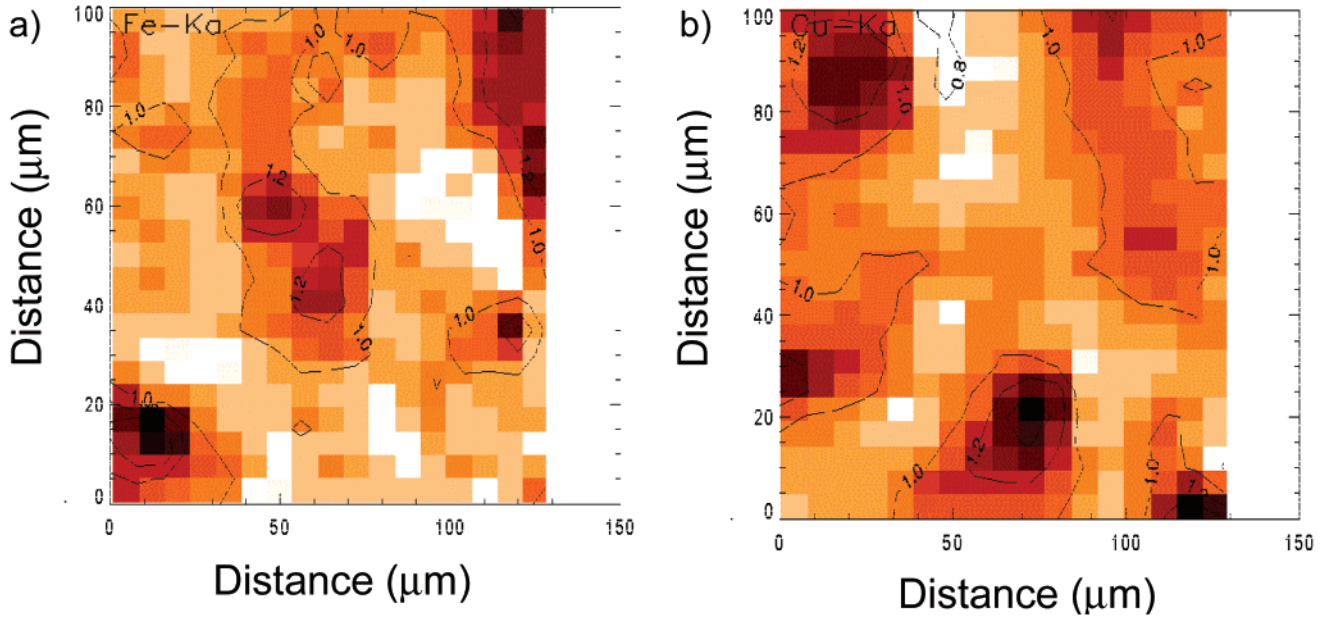


Figure 6. Spatial concentrations $c_i$ of repeated analyses for (a) Fe and (b) Cu in the NIST SRM 1577a material. White corresponds to the lowest $c_i$ value while black is the highest value. Contour plots for each $E$ value are included.

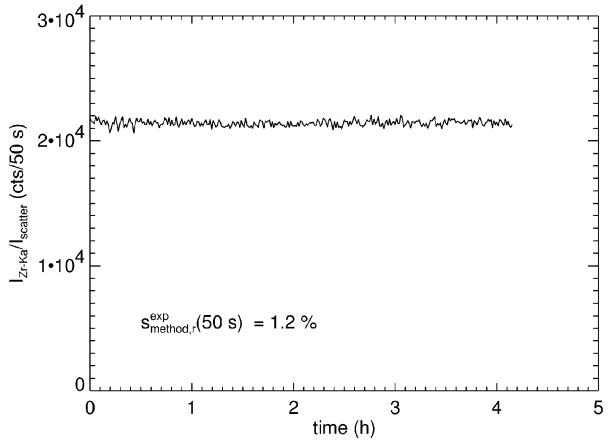


Figure 7. Experimental $I_{Zr-K\alpha}/I_{scatter}$ resulting from repeated measurements on NIST SRM 613 glass irradiated with a 5 × 8 $\mu$m$^2$ X-ray beam at the same position using a collection time of 50 s. $I_{Zr-K\alpha}$: intensity of Zr Kα fluorescent line; $I_{scatter}$: intensity of scatter background area in the X-ray spectrum. Even after prolonged irradiation, no sign of material degradation or loss of analyte is observed.

Table 2. Values of $s_{method,r}$, $s_{statistics,r}$, and $s_{instrument,r}$ Determined from 300 Repeated Measurements on a NIST SRM 613 Sample with a 50-s Measuring Time and a Step Size of 0 $\mu$m[a]

| | NIST SRM 613 (300 replicates) | | | | |
|---|---|---|---|---|---|
| | concn ($\mu$g/g) | $m$ (ng) | $s_{method,r}$ (%) | $s_{stat,r}$ (%) | $s_{instr,r}$ (%) |
| Ni | 38.8 | 39 | 11.0 | 10.7 | 2.5 |
| Cu | (37.7) | 48 | 5.0 | 4.9 | 0.8 |
| Zn | [40] | 58 | 4.3 | 4.3 | 0.5 |
| Ga | [40] | 70 | 4.0 | 4.0 | |
| Ge | [40] | 83 | 3.3 | 2.9 | 1.4 |
| Se | [40] | 115 | 3.2 | 3.0 | 1.0 |
| Rb | 31.4 | 163 | 1.7 | 1.2 | 1.1 |
| Sr | 78.4 | 163 | 1.1 | 0.7 | 0.9 |
| Y | [40] | 163 | 1.3 | 0.9 | 0.9 |
| Zr | [40] | 163 | 1.2 | 0.9 | 0.8 |
| Nb | [40] | 163 | 1.1 | 0.8 | 0.9 |
| Mo | [40] | 163 | 1.1 | 0.7 | 0.8 |
| Pb | 38.6 | 99 | 1.9 | 1.5 | 1.2 |

[a] The sampling mass $m$ is 5 ng.

and $s_{statistics,r}$. Since the net intensity $I_{fl,I}$ is obtained as the difference between the total intensity $T_{fl,i}$ in a window around the analytical X-ray peak and that of the background ($B_{fl,i}$) in that spectral window, $s^2_{statistics,r}(I_{fl,i})$ must be calculated as

$$s^2_{statistics,r}(I_{fl,i}) = s^2(T_{fl,i} - B_{fl,i}) = s^2(T_{fl,i}) + s^2(B_{fl,i}) = T_{fl,i} + B_{fl,i} = I_{fl,i} + 2B_{fl,i} \quad (6)$$

As an example, Figure 7 shows the result for Zr in a NIST SRM 613 glass sample from a series of 300 replicate analyses (performed at ESRF-ID18F) and a 50-s measuring time per analysis. The average net fluorescent intensity of Zr in the glass sample $<I_{fl,Zr}>$ equaled 21 414 counts/50 s with $s_{method,r}$ = 1.2%. The average background intensity of Zr $<B_{fl,Zr}>$ equaled 2024 counts, yielding an estimate for $s_{statistics,r}(I_{fl,Zr} + B_{fl,Zr})$ of $\{(21414 + 2 \times 2024)^{1/2}/21414] \times 100\% = 0.7\%$. Together with a variation of ~0.6% for $s_{statistics,r}(I_{scatter})$, a value of $(0.7^2 + 0.2^2)^{1/2} = 0.9\%$ for $s_{statistics,r}$ was obtained. Once $s_{statistics,r}$ was calculated using eq 5, the instrumental variation of the XRF setup $s_{instrument,r}$ could be estimated by means of eq 1. For Zr in the above-described example, $s_{instrument,r}$ equaled $(1.2^2 - 0.9^2)^{1/2} = 0.8\%$. Table 2 lists the values of $s_{method,r}$, $s_{statistics,r}$, and $s_{instrument,r}$ for a number of other elements in NIST SRM 613 obtained with the ESRF-ID18F $\mu$-XRF setup. Here we observe $s_{instrument,r}$ values of 1−2% for the elements listed in Table 2, except for Ni (among the listed elements, Ni is the least well excited by the primary X-ray beam energy of 21 keV). The irradiated mass $m_i$ for each trace element $i$ in the NIST SRM 613 sample is also listed; these values were calculated by considering the information depth of a given characteristic fluorescent line in a glass matrix ($\rho \approx 2.3$ g/cm$^3$) when 99% of

Table 3. Values of $s_{method,r}$, $s_{statistics,r}$, and $s_{instrument,r}$ Determined from 100 Repeated Measurements on a NIST SRM 1577a Sample with 50-s Measuring Time and a Step Size of 0 $\mu$m

| | NIST SRM 1577a (100 replicates) | | | | |
|---|---|---|---|---|---|
| | concn ($\mu$g/g) | $m$ (ng) | $s_{method,r}$ (%) | $s_{stat,r}$ (%) | $s_{instr,r}$ (%) |
| Mn | 10.3 | 5 | 4.6 | 4.5 | <1 |
| Fe | 270 | 5 | 3.0 | 1.4 | 2.6 |
| Cu | 193 | 5 | 2.3 | 1.4 | 1.8 |
| Zn | 130 | 5 | 1.8 | 1.4 | 1.1 |
| Rb | 18.3 | 5 | 2.2 | 1.7 | 1.3 |

the intensity is detected compared to an infinitely thick sample.[23] Additionally, elemental maps similar to those shown in Figure 6 do not reveal the presence of any enriched areas or nuggets.

An identical series of repeated measurements was performed on a NIST SRM 1577a pellet. Here, 100 replicate analyses were carried out at the ESRF-ID18F station; the resulting values of $s_{method,r}$, $s_{statistics,r}$, and $s_{instrument,r}$ for Mn, Fe, Cu, Zn, and Rb are listed in Table 3. Here we observe $s_{instrument,r}$ values of 1−3% for all the elements in the sample, resulting in $s_{method,r}$ values of <5%. Previously, we reported $s_{instrument,r}$ values of 2−4% obtained by means of repeated measurements on a NIST SRM 1577a sample for the HASYLAB $\mu$-XRF setup (beam line L).[14]

From the data listed in Tables 2 and 3, it can be concluded that by means of the ESRF-ID18F $\mu$-XRF setup and when using a 50-s data collection interval per spectrum and the data handling procedure outlined above, measurement of the heterogeneity levels of trace constituents between the 10 and 300 $\mu$g/g level in analyzed sample masses in the range of 5−160 ng is possible, provided the observed heterogeneity levels are larger than ∼5%.

The low values for $s_{instrument}$ obtained for various traces in both types of reference materials confirm the reputation of $\mu$-XRF as a "quasi-nondestructive" trace-level microanalytical methods.

**Calculation of $m_{min,5\%}$ for the Trace Metals in Homogeneous Standard NIST SRM 613.** The $m$-dependence of $s_{total,r}$(Zr), $s_{method,r}$(Zr), and $s_{material,r}$(Zr) as derived from experimental data in a NIST SRM 613 glass wafer for 0.16 $\mu$g < $m$ < 9 $\mu$g is plotted in Figure 8. When calculating $m_{min,5\%}$ for reference materials of type a and type b heterogeneity (Figure 4), it can be assumed that $s_{material,r} \propto 1/m^{1/2}$ (see Figure 3). Accordingly, to obtain the data points in Figure 8, only measurements at $m$ = 0.16 $\mu$g were performed; to calculate $s_{total,r}$(Zr), $s_{method,r}$(Zr), and $s_{material,r}$(Zr) values at 2$m$, 4$m$, etc., the original series of 441 independent X-ray intensity readings were pairwise added. From the resulting $s_{material,r}(m)$ versus $m$ graph and by means of eq 3, a value of $m_{min,5\%}$ = 16 ng for Zr analysis can be derived. The normalized experimental intensities $<I_{el}/I_{scatter}>$ and the corresponding $s_{total,r}$, $s_{method,r}$, and $m_{min,5\%}$ values for Zr and other elements in NIST SRM 613 are listed in Table 4, together with the result of a Kolmogorov−Smirnov (K−S) test for normality of the data series.[24] We can observe that most elements in the NIST SRM 613 sample are distributed in a Gaussian manner, except for Cu, Zr, and Pb. It should be noted that only when $s_{total,r}$ is significantly higher than $s_{method,r}$, can a meaningful value for $m_{min,5\%}$ be calculated

(24) Jobson, J. D. *Applied Multivariate Data Analysis*; Springer: New York, 1991; Vol. 1.

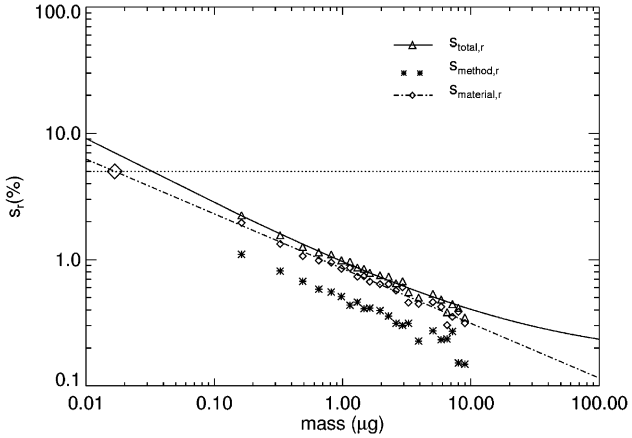


Figure 8. Log/log representation of the exponential decrease of $s_{total,r}$, $s_{method,r}$, and $s_{material,r}$ vs $m$ of $I_{Zr-K\alpha}/I_{scatter}$ in NIST SRM 613, analyzed with an X-ray beam of 5 × 8 $\mu$m$^2$.

Table 4. Values of the Normalized Intensity $<I_{el}/I_{scatt}>$, $s_{total,r}$, $s_{method,r}$, and the Minimal Representative Mass $m_{min,5\%}$ for Some Trace Elements in the NIST SRM 613 Glass Sample

| | NIST SRM 613 (441 measurements) | | | | |
|---|---|---|---|---|---|
| | $<I_{el}/I_{scatt}>$ (counts) | $s_{total,r}$ (%) | $s_{method,r}$ (%) | distr (K−S) | $m_{min,5\%}$ (ng) |
| Ni | 554 | 10.0 | 10.0 | Gaussian | ≪36 |
| Cu | 1335 | 8.1 | 4.7 | distorted | 35 |
| Zn | 1658 | 4.8 | 4.0 | Gaussian | 2 |
| Ga | 1781 | 4.3 | 4.0 | Gaussian | <40 |
| Ge | 2758 | 2.9 | 2.9 | Gaussian | ≪83 |
| Se | 2280 | 3.2 | 3.2 | Gaussian | 1 |
| Rb | 10214 | 1.7 | 1.7 | Gaussian | <10 |
| Sr | 27509 | 1.1 | 1.1 | Gaussian | ≪163 |
| Y | 16163 | 1.4 | 1.3 | Gaussian | <5 |
| Zr | 21810 | 2.2 | 1.2 | distorted | 16 |
| Nb | 24045 | 1.3 | 1.1 | Gaussian | 11 |
| Mo | 27459 | 1.2 | 1.1 | Gaussian | <6 |
| Pb | 6150 | 2.3 | 1.9 | distorted | <20 |

(see Cu, Zn, Se, Zr, and Nb in Table 4). In the other cases (see Ga, Rb, Y, Mo, and Pb), only an estimate of the upper limit for $m_{min,5\%}$ can be calculated (by setting $s_{total,r}$ equal to 5% in eq 2). When $s_{method,r}$ is almost identical to $s_{total,r}$, this indicates that the trace element is homogeneously distributed in the material and that the corresponding $m_{min,5\%}$ value is much smaller than the irradiated mass $m$ (as is the case for Ni, Ge, and Sr in Table 4). When all the $m_{min,5\%}$ values in Table 4 are considered, it can be concluded that when NIST SRM 613 is to be used for the calibration of microanalytical instruments for the elements Ni, Cu, Zn, Ga, Ge, Se, Rb, Sr, Y, Zr, Nb, Mo, and Pb, at least 100 ng of the glass material should be analyzed.

The $m_{min,5\%}$ data in Table 4 result from a single series of experimental data. The above-described Monte Carlo model was able to reproduce this experimental data set with a high degree of reliability. For example, for Zr, on the basis of the simulated data, a value of $m_{min,5\%}$ = 17 ng is obtained for Zr in NIST SRM 613, while experimentally, $m_{min,5\%}$ = 16 ng was found at $m$ = 0.14 $\mu$g (see left most data point in Figure 9). Having a realistic simulation model available, it was used to investigate the precision with with $m_{min,5\%}$ values can be determined as a function of the analyzed mass $m$. Figure 9 summarizes the results for Zr in NIST

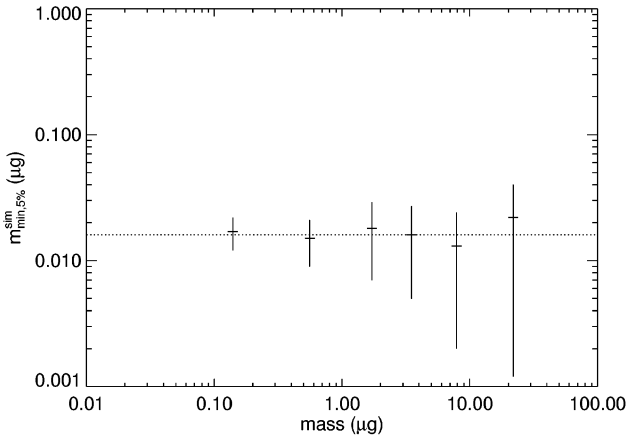


Figure 9. $m^{sim}_{min,5\%}$ values together with their uncertainty vs the analyzed mass $m$ obtained by means of a Monte Carlo simulation model constructed for Zr in NIST SRM 613 glass.

SRM 613. To determine the uncertainties on the $m^{sim}_{min,5\%}$ values, the entire simulation procedure was repeated 10 times at each $m$ value, but at different positions in the model (equivalent to the irradiation of different areas on a large sample). As shown in Figure 9, similar $m^{sim}_{min,5\%}$ values are observed when $m$ increases up to ~20 $\mu$g, albeit with increasing uncertainty. This increase is mainly due to the decreasing difference between $s_{method,r}$ and $s_{total,r}$ when $m$ is increased.

From Table 4 and Figure 9, we conclude that all detectable trace elements in the NIST SRM 612 sample are homogeneously distributed, even when a relatively small sampling mass of 0.16 $\mu$g is employed. To ensure a precise determination of $m_{min,5\%}$, it appears recommended to use a value for $m$ between 0.1 and 1 $\mu$g.

NIST SRM 613 was thus found to be suitable as a microanalytical reference material for the trace elements Ni, Cu, Zn, Ga, Ge, Se, Rb, Sr, Y, Zr, Nb, Mo, and Pb when 0.1 $\mu$g of material is being employed.

**Calculation of $m_{min,5\%}$ for the Trace Metals in Heterogeneous Standard NIST SRM 1577a.** *Structures in Elemental Maps Derived from NIST SRM 1577a.* In panels a and b of Figure 6, respectively, the autonormalized concentration maps $E(x,y) = c(x,y)/\langle c_{map}\rangle$ of Fe and Cu in NIST SRM 1577a are shown where $c(x,y)$ is the measured concentration value in pixel $(x,y)$; $E(x,y)$ and its standard deviation both are dimensionless quantities. In the case of Fe, throughout the mapped area, enrichment values with standard deviation $s_{map} = 0.13$ are obtained. Therefore, all pixels with $E > 1.4$ are considered to be nuggets (see lower left area in Figure 6a showing a nugget with $S_{nugget} \cong 10 \times 15$ $\mu$m$^2$). Several larger areas with average enrichment factors between 1.0 and 1.4 can be distinguished, having an area $S_{island} \cong 50 \times 60$ $\mu$m$^2$. Similar observations can be done in Figure 6b for Cu, although the nuggets and islands are found back at other positions and of different sizes. For Mn, Zn, and Rb, no nuggets were observed during the analyses of this SRM.

It can be concluded that when the heterogeneity of NIST SRM 1577a and similar materials are to be studied, the presence of the nuggets and islands of the above-cited dimensions needs to be taken into account.

To evaluate the microheterogeneity of the trace elements in NIST SRM 1577a, a pressed pellet of the bovine liver material was analyzed in the same way as for NIST SRM 613 described above. Experimental values for the mean intensity $\langle I_{el}/I_{scatter}\rangle$,

Table 5. Values of the Normalized Intensity $\langle I_{el}/I_{scatt}\rangle$, $s_{total,r}$, $s_{method,r}$, $s_{material,r}$, and the Result of the Kolmogorov−Smirnov Test for Normality, for Some Trace Elements in the NIST SRM 1577a Sample[a]

| | NIST SRM 1577a ($m$ = 5 ng) | | | | |
|---|---|---|---|---|---|
| | $\langle I_{el}/I_{scatt}\rangle$ (counts) | $s_{total,r}$ (%) | $s_{method,r}$ (%) | $s_{material,r}$ (%) | distr (K−S) |
| Mn | 442 | 10.9 | 4.6 | 9.9 | Gaussian |
| Fe | 15517 | 17.4 | 3.0 | 17.1 | distorted |
| Cu | 21953 | 23.2 | 2.3 | 23.1 | distorted |
| Zn | 18188 | 5.5 | 1.4 | 5.2 | distorted |
| Rb | 5585 | 5.0 | 1.9 | 4.5 | distorted |

[a] The analyzed mass $m$ Is 5 ng.

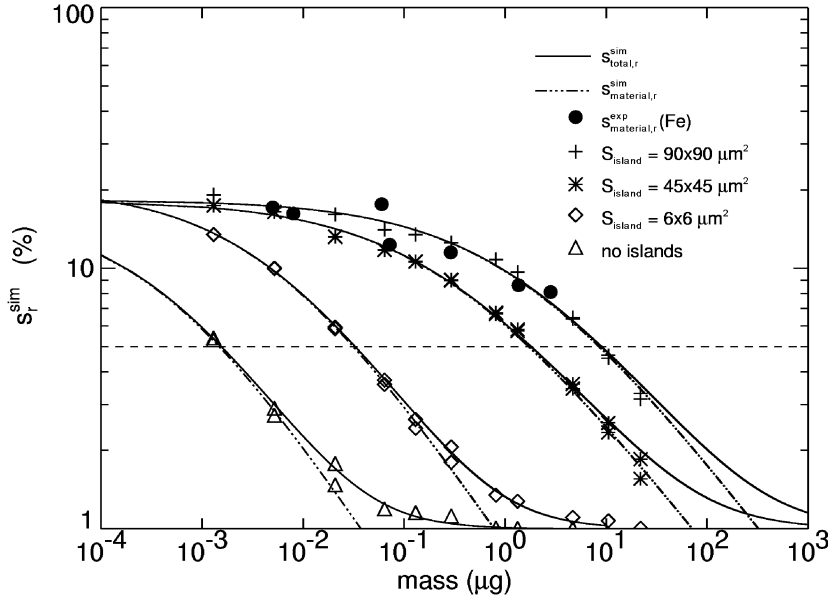


Figure 10. $s^{sim}_{total,r}$ and $s^{sim}_{material,r}$ values vs analyzed mass $m$ of Fe in the NIST SRM 1577a sample model obtained with different values for $S_{island}$, together with the experimental $s^{exp}_{material,r}$ values.

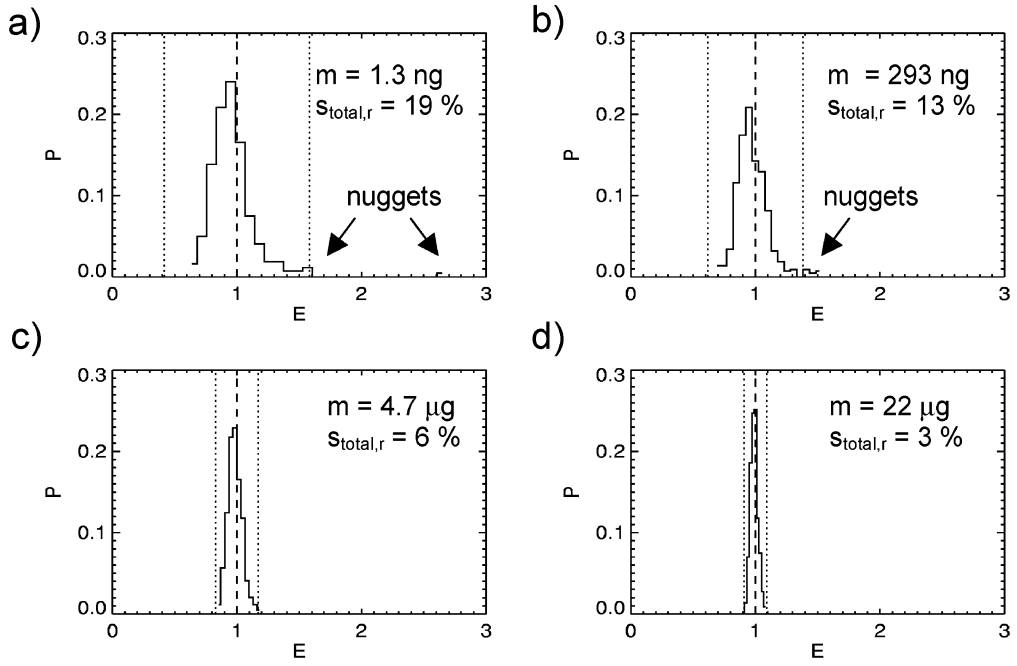


Figure 11. Frequency distributions of Fe in the NIST SRM 1577a sample model when analyzing the sample with a mass of (a) $m = 1.3$ ng, (b) $m = 293$ ng, (c) $m = 4.7$ $\mu$g, and (d) $m = 22$ $\mu$g. The $\pm 3s$ interval around $E = 1$ is also indicated, together with its $s^{sim}_{total,r}$ value.

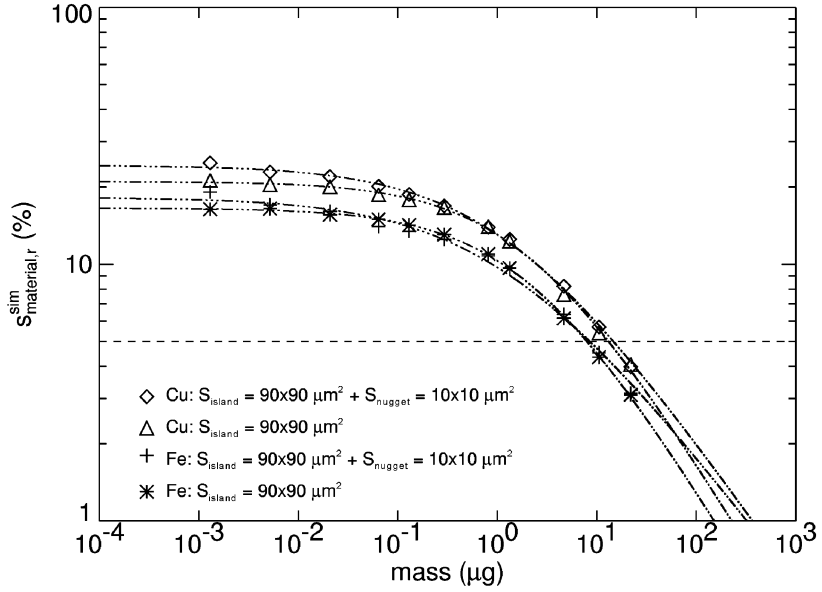


Figure 12. Comparison of $s^{sim}_{material,r}$ vs $m$ values of Fe and Cu in the NIST SRM 1577a material with and without nuggets present in the sample model.

$s_{total,r}$, $s_{method,r}$, and $s_{material,r}$, together with the result of a K−S test for normality are listed in Table 5 for several trace elements. We observe that only the Mn concentration throughout the material is normally distributed while the Rb data show a value for $s_{material,r}$ below 5%. From this we conclude that, at the 95% confidence level, Rb is distributed homogeneously in the material when 5 ng is analyzed during each measurement. Mn, Fe Cu, and Zn on the other hand are distributed heterogeneously in the NIST SRM 1577a sample.

To investigate the nature of the microheterogeneity of Fe, a Monte Carlo model was constructed by randomly distributing nuggets and islands in the model with $S_{nugget} = 10 \times 10$ $\mu$m$^2$ and islands of different sizes; the size and enrichtment factor of the islands were set to values observed in experimentally recorded distributions (see Figure 6). In Figure 10, the resulting variation of $s^{sim}_{total,r}$(Fe) and $s^{sim}_{material,r}$(Fe) for 0.001 $\mu$g < $m$ < 22 $\mu$g is plotted. Depending on the parameters of the inclusions that were used as input to the MC model, different $s^{sim}_{total,r}$ and $s^{sim}_{material,r}$ versus $m$ curves are obtained. Fairly large islands are required as part of the simulation model to allow reproduction of the experimental data.

Figure 11 shows the corresponding histograms for the distributions with $m = 1.3$, 293, 4.7, and ~22 $\mu$g, together with their $s^{sim}_{total,r}$ value for Fe in NIST SRM 1577a sample model. In Figure 11a, an asymmetric main distribution can be observed, with a few well-separated nuggets visible, resulting in a high $s^{sim}_{total,r}$ value. When the analyzed mass $m$ increases, the probability $P$ to observe a nugget and the enrichment value $E$ of those nuggets decreases,

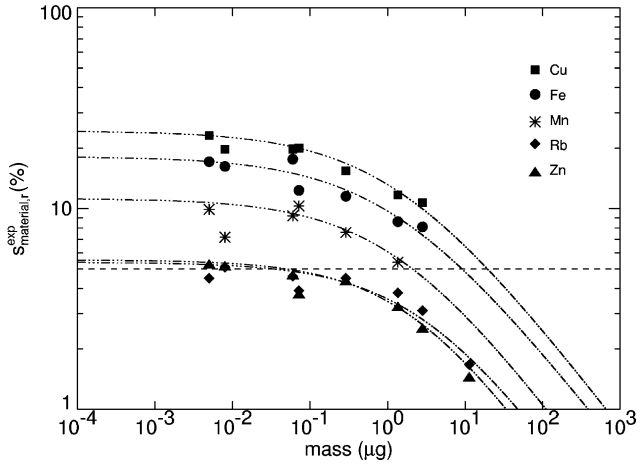


Figure 13. $s^{exp}_{material,r}$ vs $m$ values obtained from experimental data for various trace elements in NIST SRM 1577a, together with its fitted simulation result.

resulting in lower $s^{sim}_{total,r}$ values. When $m$ is sufficient large (see Figure 11d), a Gaussian-like distribution is obtained.

Next to the effect of the island dimensions on $m_{min,5\%}$, the influence of the presence of nuggets was also investigated: Fe and Cu data series were simulated with and without nuggets being present using $S_{island} \cong 90 \times 90\ \mu m^2$. In Figure 12, the resulting $m^{sim}_{min,5\%}$ values are plotted versus $m$. Only slightly lower $m^{sim}_{min,5\%}$ values are obtained when no nuggets are taken into consideration than in the case where they are present in the model.

From Figure 10 and Figure 12, we conclude that the dependency of $m^{sim}_{min,5\%}$ on $m$ is mainly due to the presence of gradual concentration variations (i.e., islands) in the sample and that the influence of abrupt and highly localized concentration variation (i.e., nuggets) on the estimated $m_{min,5\%}$ values is only of secondary importance when large series of independent measurements are performed.

In Figure 13, the $s_{material,r}$ values obtained by repeated analysis of NIST SRM 1577a using different X-ray microbeam sizes, corresponding to $0.008\ \mu g < m < 2.83\ \mu g$ (see Figure 2), are plotted versus $m$ for the elements Mn, Fe, Cu, Zn, and Rb (symbols) and compared to simulated data (lines). As predicted by the simulation, for all the trace elements in the sample, a dependency of $s_{material,r}$ on $m$ is observed that clearly deviates from $1/m^{1/2}$.

When comparing both experimental and simulated results for Fe (see Figure 10), we observe an under- or overestimation of the $s_{material,r}$ versus $m$ values when a simulation model with incorrect island size is employed. The best matching result for Fe in the NIST SRM 1577a sample is obtained when islands with $S_{island} \cong 90 \times 90\ \mu m^2$ are employed in the sample model. The best matching input parameters of $S_{nugget}$ and $S_{island}$ for Fe, Mn, Cu, Zn, and Rb are listed in Table 6 together with the average intensity $<I_{el}>$ of the model, the instrumental variation $s_{instrument,r}$, and the corresponding $F = (s^{exp}_{total,r})^2/(s^{sim}_{total,r})^2$ values. The best matching island sizes result from $S_{island} \cong 90 \times 90\ \mu m^2$ for Mn, Fe, and Cu to $S_{island} \cong 210 \times 210\ \mu m^2$ for Rb. For all the elements in the model (except for Mn), small nuggets with $S_{nugget} = 10 \times 10\ \mu m^2$ were employed as part of the model, in accordance with the experimental results. For all the elements listed in Table 6, calculated $F$ values lower than the critical $F$ value (equal to 1.17) are obtained, indicating that both experimental and simulated distributions are similar. It can be concluded that, in case of the heterogeneous NIST SRM 1577a, the Monte Carlo simulation model is able to predict the experimental observed $s_{material,r}$ values.

Table 6. Input Parameters $S_{island}$, $S_{nugget}$, $<I_{el}>$, and $s_{instrument,r}$ for the Monte Carlo Simulation Model of Some Trace Elements in the NIST SRM 1577a Sample, Together with the Result of the $F$ Test and the Calculated $m_{min,5\%}$

| | NIST SRM 1577a | | | | | |
|---|---|---|---|---|---|---|
| | $S_{island}$ ($\mu m^2$) | $S_{nugget}$ ($\mu m^2$) | $<I_{el}>$ (counts) | $s_{instr,r}$ (%) | $F$ value | $m_{min,5\%}$ ($\mu g$) |
| Mn | 90 × 90 | | 463 | 1 | 1.14 | 2.1 |
| Fe | 90 × 90 | 10 × 10 | 15435 | 1 | 1.11 | 9.1 |
| Cu | 90 × 90 | 10 × 10 | 22240 | 1 | 1.12 | 19.4 |
| Zn | 120 × 120 | 10 × 10 | 18443 | 1 | 1.13 | 0.05 |
| Rb | 210 × 210 | 10 × 10 | 5505 | 1 | 1.16 | 0.03 |

Once the best-fitting parameters for each element in the model are obtained (see parameters listed in Table 6 and lines in Figure 13), $m_{min,5\%}$ can be calculated. Values of $m_{min,5\%}$ for the trace elements in NIST SRM 1577a are also listed in Table 6. When considering the $m_{min,5\%}$ values in Table 6, it can be concluded that when NIST SRM 1577a is to be used for the calibration of microanalytical instruments for the elements Mn, Fe, Cu, Zn, and Rb, at least 20 $\mu g$ of material must be analyzed. Still, these values are considerably lower than the minimal representative mass indicated on the certificate (250 mg).

Received for review March 28, 2002. Revised manuscript received July 13, 2002. Accepted July 24, 2002.

AC025662G